

Alma Mater Studiorum Università di Bologna
Archivio istituzionale della ricerca

Analytical solution of cross- and angle-ply nano plates with strain gradient theory for linear vibrations and buckling

This is the final peer-reviewed author's accepted manuscript (postprint) of the following publication:

Published Version:

Cornacchia, F., Fabbrocino, F., Fantuzzi, N., Luciano, R., Penna, R. (2021). Analytical solution of cross- and angle-ply nano plates with strain gradient theory for linear vibrations and buckling. *MECHANICS OF ADVANCED MATERIALS AND STRUCTURES*, 28(12), 1201-1215 [10.1080/15376494.2019.1655613].

Availability:

This version is available at: <https://hdl.handle.net/11585/698729> since: 2024-09-19

Published:

DOI: <http://doi.org/10.1080/15376494.2019.1655613>

Terms of use:

Some rights reserved. The terms and conditions for the reuse of this version of the manuscript are specified in the publishing policy. For all terms of use and more information see the publisher's website.

This item was downloaded from IRIS Università di Bologna (<https://cris.unibo.it/>).
When citing, please refer to the published version.

(Article begins on next page)

Analytical solution of cross- and angle-ply nano plates with strain gradient theory for linear vibrations and buckling

F. Cornacchia¹, F. Fabbrocino², N. Fantuzzi¹, R. Luciano^{3,*}, R. Penna⁴

Abstract

Vibrations and buckling of Kirchhoff nano plates are investigated using second-order strain gradient theory. The Navier displacement field has been considered for two different sets of boundary conditions and stacking sequences. Different geometries and material properties for isotropic, orthotropic cross- and angle-ply laminates are considered, and numerical simulations are discussed in terms of plate aspect ratio and non local ratio. A comparison with the classical analytical solution is provided whenever possible for buckling loads and fundamental frequencies.

Keywords: Stability analysis, Dynamic analysis, Orthotropic laminate, Nano-structures, Nonlocal elastic theory, Analytical modelling

1. Introduction

2 In the current literature MEMS (Micro-Electro-Mechanical-System) and
3 NEMS (Nano-Electro-Mechanical-System) are topics of relevant interest be-

*raimondo.luciano@uniparthenope.it

¹DICAM Department University of Bologna, Italy

²Engineering Department, Pegaso Telematic University, Italy

³Engineering Department, Parthenope University, Italy

⁴Department of Civil Engineering, University of Salerno, Italy

4 cause of their various uses [1, 2, 3]. Indeed, these types of materials can be
5 employed in many areas of application, i.e. engineering, medicine and elec-
6 tronics [4, 2, 5, 6, 7], in the form of generators, transistors, sensors, actuators,
7 resonators, detectors etc.

8 This work wants to focus the attention on NEMS, which are usually mod-
9 eled by simulating small scale effects on nano rods, nano beams, nano tubes
10 and nano plates. In fact, the mechanical behavior of nano structural com-
11 ponents is size-dependent [8, 9, 10, 11, 12], highly influenced by the material
12 structure and by the interactions at the atomic scale among particles at dis-
13 tant location, as commented in [13, 14, 15, 16, 17, 18, 19, 20, 21], effects that
14 have much lower impact in macro structures. Thus, in order to take into
15 account the size effects, the classical continuum mechanics theories are not
16 suitable, which implies the application of modified versions [22, 23, 24, 25],
17 that are based on the individuation of an internal length scale. A wide range
18 of non classical theories have been developed in order to capture the non
19 locality effects, among which Eringen [26, 26] was one of the pioneer and his
20 nonlocal elasticity theory has been extensively applied in the study of nano
21 structures by scientists [27, 28, 29]. Hence, an important milestone in the
22 practice of higher order theories of linear elasticity is to determine the cor-
23 rect non local relation [30, 31]. A broad list of higher order theories of linear
24 elasticity can be found in literature, among which, strain gradient, modified
25 strain gradient, stress gradient, modified couple stress and micropolar the-
26 ories can be identified [32? , 33, 25, 34, 35, 36, 37, 38, 39], and the choice
27 depends on the research to carry out and on the ability of the scientists.
28 Here, the effort will be focused on the development of studies of buckling

29 and vibrations of nano plates, which is a relevant subject for the scientific
30 community, as it can be found in [40, 41, 42, 43, 44, 45, 46, 47, 48, 49]. An
31 easy theory, which is applied in the present study, is the second order-strain
32 gradient theory that establish a connection between stress and strain of the
33 structure in the constitutive equations through a single non local parameter,
34 as previously done by Papargyri-Beskos [50]. The method followed in the
35 present paper follows the one presented in [51] for static analysis of lami-
36 nates, where the gap between the theories in terms of deflection and stresses
37 is shown. In fact, the Kirchhoff governing equations in weak form are car-
38 ried out by considering the size effects, while the Navier displacement field is
39 applied in order to develop the analytical solution in terms of stability and
40 dynamic analysis. Comparison with Reddy [52], Papargyri-Beskos [50] and
41 Babu Patel [21] are provided if possible for the classical continuum mechanics
42 theory, before extending the application to orthotropic laminated materials
43 (cross- and angle-ply laminates) employing the second order-strain gradient
44 theory.

45 **2. Theoretical model**

46 *2.1. Kirchhoff theory*

47 Different combinations of geometrical and material configurations of or-
48 thotropic thin rectangular nanoplates are implemented by making use of the
49 classical laminated plate theory (CLPT). In order to conduct stability and
50 dynamic analysis for such structures, at nano scale level, a modification of the
51 theory, based on the bending plate hypothesis of Kirchhoff is needed. The
52 laminates have dimension a and b along x - and y -axis, respectively, while

53 the thickness of the generic oriented k -th lamina $h_k = z_{k+1} - z_k$, as it is
54 displayed in Fig. 1 For the case of geometric non linearity, the displacements
55 in the three directions can be written from the Kirchhoff assumptions and
56 restrictions as it follows:

$$\begin{aligned}
u(x, y, z, t) &= u_0(x, y, t) - zw_{0,x} \\
v(x, y, z, t) &= v_0(x, y, t) - zw_{0,y} \\
w(x, y, z, t) &= w_0(x, y, t)
\end{aligned} \tag{1}$$

57 where, u_0, v_0, w_0 are the displacements along x -, y - and z -axis of the points
58 on the mid-surface, and $w_{0,x}$ and $w_{0,y}$ are the homologous rotations.

59 The plate strain is expressed in the von Karman form:

$$\varepsilon = \{\varepsilon^{(m)}\} + z \{\varepsilon^{(f)}\} = \begin{Bmatrix} \varepsilon_{xx}^{(m)} \\ \varepsilon_{yy}^{(m)} \\ \gamma_{xy}^{(m)} \end{Bmatrix} + z \begin{Bmatrix} \varepsilon_{xx}^{(f)} \\ \varepsilon_{yy}^{(f)} \\ \gamma_{xy}^{(f)} \end{Bmatrix} \tag{2}$$

60 where, $^{(m)}$ indicates the membrane strain, while $^{(f)}$ the flexural strain. ε_{xx}
61 and ε_{yy} are the normal strains along x and y directions respectively, instead
62 γ_{xy} represents the in-plane shear strain. Consequently, the membrane and
63 flexural strains can be written as function of the displacements:

$$\begin{Bmatrix} \varepsilon_{xx}^{(m)} \\ \varepsilon_{yy}^{(m)} \\ \gamma_{xy}^{(m)} \end{Bmatrix} = \begin{bmatrix} u_{0,x} + \frac{1}{2}w_{0,x}^2 \\ v_{0,y} + \frac{1}{2}w_{0,y}^2 \\ u_{0,y} + v_{0,x} + w_{0,x} w_{0,y} \end{bmatrix}, \quad \begin{Bmatrix} \varepsilon_{xx}^{(f)} \\ \varepsilon_{yy}^{(f)} \\ \gamma_{xy}^{(f)} \end{Bmatrix} = \begin{bmatrix} -w_{0,xx} \\ -w_{0,yy} \\ -2w_{0,xy} \end{bmatrix} \tag{3}$$

64 In order to take into account the effects of non locality due to the di-
65 mensions of the nano plates, the second-order strain gradient theory must

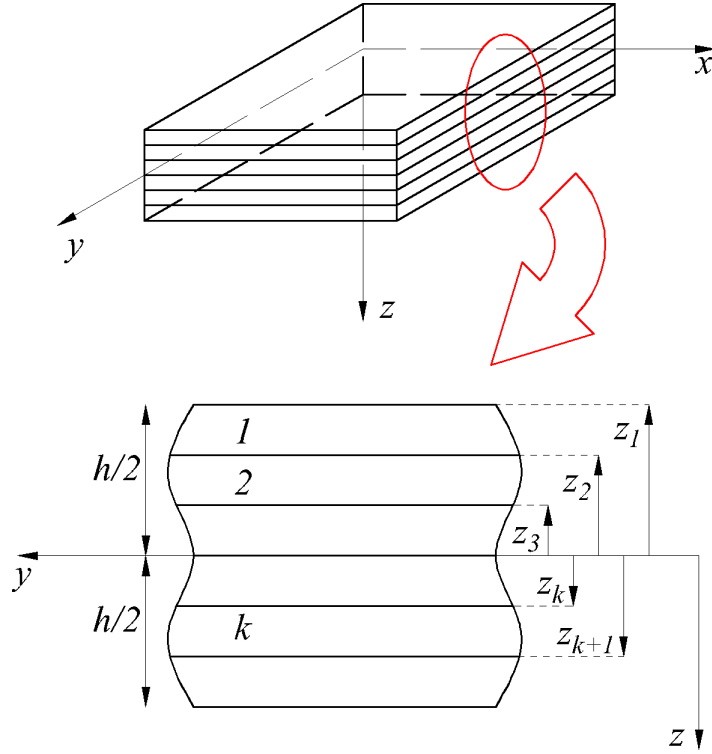


Figure 1: Laminate general layout

66 be involved in the computation. For the k -th orthotropic lamina in terms of
 67 laminate coordinates, the constitutive equations can be written as:

$$\begin{Bmatrix} \sigma_{xx} \\ \sigma_{yy} \\ \tau_{xy} \end{Bmatrix}^{(k)} = (1 - \ell^2 \nabla^2) \begin{bmatrix} \bar{Q}_{11} & \bar{Q}_{12} & \bar{Q}_{16} \\ \bar{Q}_{12} & \bar{Q}_{22} & \bar{Q}_{26} \\ \bar{Q}_{16} & \bar{Q}_{26} & \bar{Q}_{66} \end{bmatrix}^{(k)} \begin{Bmatrix} \varepsilon_{xx} \\ \varepsilon_{yy} \\ \gamma_{xy} \end{Bmatrix}^{(k)} \quad (4)$$

68 where, $\nabla^2 = \partial^2/\partial y^2 + \partial^2/\partial x^2$, and \bar{Q}_{ij} are function of sheets orienta-
 69 tions and are derived from the engineering constants in accordance with the

70 formulations below:

$$\begin{aligned} Q_{11} &= \frac{E_1}{1 - \nu_{12}\nu_{21}}, & Q_{22} &= \frac{E_2}{1 - \nu_{12}\nu_{21}} \\ Q_{12} &= \frac{E_1\nu_{21}}{1 - \nu_{12}\nu_{21}} = \frac{E_2\nu_{12}}{1 - \nu_{12}\nu_{21}}, & Q_{66} &= G_{12} \end{aligned} \quad (5)$$

71 where, E_1 , E_2 are the Young's moduli, ν_{12} and ν_{21} are the Poisson's ratios
72 and G_{12} is the shear modulus.

73 The dynamic version of the principle of the virtual works (Hamilton's
74 Principle) is employed in order to carry out the equations of motion. It
75 is important to point out that the transverse shear stress, needed for the
76 equilibrium of the plate, has been involved in the boundary conditions and
77 equilibrium of forces.

$$\int_0^T (\delta U + \delta V - \delta K) = 0 \quad (6)$$

78 with, δU is the virtual strain energy, δV is the virtual work done by the
79 applied forces, and δK is the virtual kinetic energy

80 Developing the terms in Eq. (6), the Hamilton's Principle can be conve-

81 niently written in extended matrix form as:

$$\begin{aligned}
& \int_0^T \int_{\Omega_0} \left[\begin{array}{c} \delta u_{0,x} \\ \delta u_{0,y} \\ \delta v_{0,x} \\ \delta v_{0,y} \\ \delta w_{0,xx} \\ \delta w_{0,yy} \\ \delta w_{0,xy} \end{array} \right]^T \begin{bmatrix} \mathcal{T}_{11} & \mathcal{T}_{12} & \mathcal{T}_{13} \\ \mathcal{T}_{21} & \mathcal{T}_{22} & \mathcal{T}_{23} \\ \mathcal{T}_{31} & \mathcal{T}_{32} & \mathcal{T}_{33} \\ \mathcal{T}_{41} & \mathcal{T}_{42} & \mathcal{T}_{43} \\ \mathcal{T}_{51} & \mathcal{T}_{52} & \mathcal{T}_{53} \\ \mathcal{T}_{61} & \mathcal{T}_{62} & \mathcal{T}_{63} \\ \mathcal{T}_{71} & \mathcal{T}_{72} & \mathcal{T}_{73} \end{bmatrix} \begin{array}{c} u_0 \\ v_0 \\ w_0 \end{array} \\
& - \left\{ \delta w_{0,x} \quad \delta w_{0,y} \right\} \begin{bmatrix} \hat{N}_{xx} & \hat{N}_{xy} \\ \hat{N}_{xy} & \hat{N}_{yy} \end{bmatrix} \begin{array}{c} w_{0,x} \\ w_{0,y} \end{array} \quad (7) \\
& + \left\{ \begin{array}{c} \delta \ddot{u}_0 \\ \delta \ddot{v}_0 \\ \delta \ddot{w}_0 \\ \delta \ddot{w}_{0,x} \\ \delta \ddot{w}_{0,y} \end{array} \right\}^T \begin{bmatrix} I_0 & 0 & 0 & -I_1 & 0 \\ 0 & I_0 & 0 & 0 & -I_1 \\ 0 & 0 & I_0 & 0 & 0 \\ -I_1 & 0 & 0 & I_2 & 0 \\ 0 & -I_1 & 0 & 0 & I_2 \end{bmatrix} \begin{array}{c} u_0 \\ v_0 \\ w_0 \\ w_{0,x} \\ w_{0,y} \end{array} \Big] dx dy \Big] dt \\
& + \text{boundary integral terms} = 0
\end{aligned}$$

82 where the variational form of the displacement field is identified by δ , while
83 its corresponding derivatives in time by the dots, the terms \mathcal{T} are shown in
84 the appendix, $\hat{N}_{xx}, \hat{N}_{yy}, \hat{N}_{xy}$ identify the axial and shear buckling terms and
85 I_0, I_1, I_2 are the mass inertias which can be defined as it follows:

$$I_i = \rho \sum_{k=1}^N \int_{z_k}^{z_{k+1}} z^i dz \quad (8)$$

86 where, $i = 0, 1, 2$. The following resultants of forces and moments are

87 obtained by integrating the stresses for each layer through the z -axis:

$$\begin{pmatrix} N_{xx} \\ N_{yy} \\ N_{xy} \end{pmatrix} = (1 - \ell^2 \nabla^2) \left(\begin{bmatrix} A_{11} & A_{12} & A_{16} \\ A_{12} & A_{22} & A_{26} \\ A_{16} & A_{26} & A_{66} \end{bmatrix} \begin{pmatrix} \varepsilon_{xx}^{(m)} \\ \varepsilon_{yy}^{(m)} \\ \gamma_{xy}^{(m)} \end{pmatrix} + \begin{bmatrix} B_{11} & B_{12} & B_{16} \\ B_{12} & B_{22} & B_{26} \\ B_{16} & B_{26} & B_{66} \end{bmatrix} \begin{pmatrix} \varepsilon_{xx}^{(f)} \\ \varepsilon_{yy}^{(f)} \\ \gamma_{xy}^{(f)} \end{pmatrix} \right) \quad (9)$$

$$\begin{pmatrix} M_{xx} \\ M_{yy} \\ M_{xy} \end{pmatrix} = (1 - \ell^2 \nabla^2) \left(\begin{bmatrix} B_{11} & B_{12} & B_{16} \\ B_{12} & B_{22} & B_{26} \\ B_{16} & B_{26} & B_{66} \end{bmatrix} \begin{pmatrix} \varepsilon_{xx}^{(m)} \\ \varepsilon_{yy}^{(m)} \\ \gamma_{xy}^{(m)} \end{pmatrix} + \begin{bmatrix} D_{11} & D_{12} & D_{16} \\ D_{12} & D_{22} & D_{26} \\ D_{16} & D_{26} & D_{66} \end{bmatrix} \begin{pmatrix} \varepsilon_{xx}^{(f)} \\ \varepsilon_{yy}^{(f)} \\ \gamma_{xy}^{(f)} \end{pmatrix} \right) \quad (10)$$

89 where, the stiffnesses are computed as it follows:

$$\begin{aligned} A_{ij} &= \sum_{k=1}^N \bar{Q}_{ij}^{(k)} (z_{k+1} - z_k) \\ B_{ij} &= \frac{1}{2} \sum_{k=1}^N \bar{Q}_{ij}^{(k)} (z_{k+1}^2 - z_k^2) \\ D_{ij} &= \frac{1}{3} \sum_{k=1}^N \bar{Q}_{ij}^{(k)} (z_{k+1}^3 - z_k^3) \end{aligned} \quad (11)$$

90 The linear equations of motion of the classical laminated plate theory
 91 in terms of displacement, accounting for non local effects are obtained by
 92 setting the non linear terms equal to zero and by carrying out integration by
 93 parts in (7):

$$\begin{aligned}
& A_{11}u_{0,xx} + 2A_{16}u_{0,xy} + A_{66}u_{0,yy} + A_{16}v_{0,xx} + (A_{12} + A_{66})v_{0,xy} + A_{26} \\
& v_{0,yy} - [B_{11}w_{0,xxx} + 3B_{16}w_{0,xxxy} + (B_{12} + 2B_{66})w_{0,xyy} + B_{26}w_{0,yyy}] - \ell^2 [A_{11} \\
& (u_{0,xxxx} + u_{0,xxyy}) + 2A_{16}(u_{0,xxxy} + u_{0,xyyy}) + A_{66}(u_{0,xyyy} + u_{0,yyyy}) + A_{16} \\
& (v_{0,xxxx} + v_{0,xxyy}) + (A_{12} + A_{66})(v_{0,xxxy} + v_{0,xyyy}) + A_{26}(v_{0,xyyy} + v_{0,yyyy}) - \\
& - [B_{11}(w_{0,xxxx} + w_{0,xxxy}) + 3B_{16}(w_{0,xxxxy} + w_{0,xxyyy}) + (B_{12} + 2B_{66}) \\
& (w_{0,xxxyy} + w_{0,xyyyy}) + B_{26}(w_{0,xyyyy} + w_{0,yyyyy})]] = I_0\ddot{u}_0 - I_1\ddot{w}_{0,x}
\end{aligned} \tag{12}$$

94

$$\begin{aligned}
& A_{16}u_{0,xx} + (A_{12} + A_{66})u_{0,xy} + A_{26}u_{0,yy} + A_{66}v_{0,xx} + 2A_{26}v_{0,xy} + A_{22} \\
& v_{0,yy} - [B_{16}w_{0,xxx} + (B_{12} + 2B_{66})w_{0,xxxy} + 3B_{26}w_{0,xyy} + B_{22}w_{0,yyy}] - \ell^2 [A_{16} \\
& (u_{0,xxxx} + u_{0,xxyy}) + (A_{12} + A_{66})(u_{0,xxxy} + u_{0,xyyy}) + A_{26}(u_{0,xyyy} + u_{0,yyyy}) + \\
& + A_{66}(v_{0,xxxx} + v_{0,xxyy}) + 2A_{26}(v_{0,xxxy} + v_{0,xyyy}) + A_{22}(v_{0,xyyy} + v_{0,yyyy}) - \\
& - [B_{16}(w_{0,xxxx} + w_{0,xxxy}) + (B_{12} + 2B_{66})(w_{0,xxxxy} + w_{0,xxyyy}) + 3B_{26} \\
& (w_{0,xxxyy} + w_{0,xyyyy}) + B_{22}(w_{0,xyyyy} + w_{0,yyyyy})]] = I_0\ddot{v}_0 - I_1\ddot{w}_{0,y}
\end{aligned} \tag{13}$$

$$\begin{aligned}
& B_{11}u_{0,xxx} + 3B_{16}u_{0,xxxy} + (B_{12} + 2B_{66})u_{0,xyy} + B_{26}u_{0,yyy} + B_{16}v_{0,xxx} + (B_{12} + \\
& + 2B_{66})v_{0,xxxy} + 3B_{26}v_{0,xyy} - B_{22}v_{0,yyy} - [D_{11}w_{0,xxxx} + 4D_{16}w_{0,xxxxy} + 2(D_{12} + \\
& + 2D_{66})w_{0,xxxy} + 4D_{26}w_{0,xyyy} + D_{22}w_{0,yyyy}] - \ell^2 [B_{11}(u_{0,xxxxx} + u_{0,xxxxy}) + \\
& + 3B_{16}(u_{0,xxxxy} + u_{0,xxxyy}) + (B_{12} + 2B_{66})(u_{0,xxxyy} + u_{0,yyyyy}) + B_{26} \\
& (u_{0,xyyyy} + u_{0,yyyyy}) + B_{16}(v_{0,xxxxx} + v_{0,xxxxy}) + (B_{12} + 2B_{66})(v_{0,xxxxy} + \\
& + v_{0,xxxyy}) + 3B_{26}(v_{0,xxxyy} + v_{0,xyyyy}) + B_{22}(v_{0,xyyyy} + v_{0,yyyyy}) - [D_{11} \\
& (w_{0,xxxxxx} + w_{0,xxxxyy}) + 4D_{16}(w_{0,xxxxyy} + w_{0,xxxyyy}) + 2(D_{12} + 2D_{66}) \\
& (w_{0,xxxyyy} + w_{0,xyyyy}) + 4D_{26}(w_{0,xxxyyy} + w_{0,xyyyy}) + D_{22}(w_{0,xyyyy} + \\
& + w_{0,yyyyy})]] = I_1(\ddot{u}_{0,x} + \ddot{v}_{0,y}) + I_0\ddot{w}_0 - I_2(\ddot{w}_{0,xx} + \ddot{w}_{0,yy}) - (\hat{N}_{xx}w_{0,xx} + \\
& + 2\hat{N}_{xy}w_{0,xy} + \hat{N}_{yy}w_{0,yy})
\end{aligned} \tag{14}$$

96 2.2. Navier solution

97 In this section, the Navier procedure for simply supported laminates is
98 applied to orthotropic cross ply and angle ply laminates. By replacing the
99 Navier displacement field, which will be made explicit in the corresponding
100 subsections, in the system below (omitting the von Karman non linear terms)
101 the analytical solutions are obtained:

$$\begin{bmatrix} \hat{c}_{11} & \hat{c}_{12} & \hat{c}_{13} \\ \hat{c}_{12} & \hat{c}_{22} & \hat{c}_{23} \\ \hat{c}_{13} & \hat{c}_{23} & \hat{c}_{33} + \hat{s}_{33} \end{bmatrix} \begin{Bmatrix} U_{mn} \\ V_{mn} \\ W_{mn} \end{Bmatrix} + \begin{bmatrix} \hat{m}_{11} & 0 & \hat{m}_{13} \\ 0 & \hat{m}_{22} & \hat{m}_{23} \\ \hat{m}_{13} & \hat{m}_{23} & \hat{m}_{33} \end{bmatrix} \begin{Bmatrix} \ddot{U}_{mn} \\ \ddot{V}_{mn} \\ \ddot{W}_{mn} \end{Bmatrix} = \begin{Bmatrix} 0 \\ 0 \\ 0 \end{Bmatrix} \tag{15}$$

102 where, the terms in the matrices will be made explicit for cross- and
103 angle-ply laminates.

104 The analytical solutions for the stability and dynamic analysis respec-
 105 tively, are carried out and shown below:

$$\bar{N} = \frac{1}{\alpha^2 + k\beta^2} \left(\hat{c}_{33} + \hat{c}_{13} \frac{a_1}{a_0} + \hat{c}_{23} \frac{a_2}{a_0} \right) \quad (16)$$

$$\bar{\omega}^2 = \frac{1}{\hat{m}_{33}} \left(\hat{c}_{33} + \hat{c}_{13} \frac{a_1}{a_0} + \hat{c}_{23} \frac{a_2}{a_0} \right) \quad (17)$$

106 where

$$\begin{aligned} a_{mn} &= \hat{c}_{33} + \hat{c}_{13} \frac{a_1}{a_0} + \hat{c}_{23} \frac{a_2}{a_0} \\ a_0 &= \hat{c}_{11}\hat{c}_{22} - \hat{c}_{12}\hat{c}_{12} \\ a_1 &= \hat{c}_{12}\hat{c}_{23} - \hat{c}_{13}\hat{c}_{22} \\ a_2 &= \hat{c}_{13}\hat{c}_{12} - \hat{c}_{11}\hat{c}_{23} \end{aligned} \quad (18)$$

107 *2.2.1. Antisymmetric Cross-Ply Laminates*

108 The Navier displacement field is assumed to be:

$$\begin{aligned} u_0(x, y) &= \sum_{n=1}^{\infty} \sum_{m=1}^{\infty} U_{mn} \cos \alpha x \sin \beta y \\ v_0(x, y) &= \sum_{n=1}^{\infty} \sum_{m=1}^{\infty} V_{mn} \sin \alpha x \cos \beta y \\ w_0(x, y) &= \sum_{n=1}^{\infty} \sum_{m=1}^{\infty} W_{mn} \sin \alpha x \sin \beta y \end{aligned} \quad (19)$$

109 where, $\alpha = m\pi/a$ and $\beta = n\pi/b$

110 in order to satisfy the displacement boundary conditions (SS-1), as it
 111 follows:

$$\begin{aligned}
u_0(x, 0, t) = 0, u_0(x, b, t) = 0, v_0(0, y, t) = 0, v_0(a, y, t) = 0 \\
w_0(x, 0, t) = 0, w_0(x, b, t) = 0, w_0(0, y, t) = 0, w_0(a, y, t) = 0 \quad (20) \\
\frac{\partial w_0}{\partial x} \Big|_{(x,0,t)} = 0, \frac{\partial w_0}{\partial x} \Big|_{(x,b,t)} = 0, \frac{\partial w_0}{\partial y} \Big|_{(0,y,t)} = 0, \frac{\partial w_0}{\partial y} \Big|_{(a,y,t)} = 0,
\end{aligned}$$

112 The coefficients to be used in Eq. (15), for the cross-ply laminate case
113 are shown below:

$$\begin{aligned}
\hat{c}_{11} &= -(\alpha^2 A_{11} + \beta^2 A_{66}) - \ell^2[\alpha^4 A_{11} + \alpha^2 \beta^2 (A_{11} + A_{66}) + \beta^4 A_{66}] \\
\hat{c}_{12} &= -\alpha\beta(A_{12} + A_{66}) - \ell^2[\alpha^3 \beta (A_{12} + A_{66}) + \alpha\beta^3 (A_{12} + A_{66})] \\
\hat{c}_{13} &= [\alpha^3 B_{11} + \alpha\beta^2 (B_{12} + 2B_{66})] + \ell^2[\alpha^5 B_{11} + \alpha^3 \beta^2 (B_{11} + B_{12} + 2B_{66}) + \\
&\quad + \alpha\beta^4 (B_{12} + 2B_{66})] \\
\hat{c}_{22} &= -(\alpha^2 A_{66} + \beta^2 A_{22}) - \ell^2[\alpha^4 A_{66} + \alpha^2 \beta^2 (A_{22} + A_{66}) + \beta^4 A_{22}] \\
\hat{c}_{23} &= [\beta^3 B_{22} + \alpha^2 \beta (B_{12} + 2B_{66})] + \ell^2[\beta^5 B_{22} + \alpha^2 \beta^3 (B_{22} + B_{12} + 2B_{66}) + \\
&\quad + \alpha^4 \beta (B_{12} + 2B_{66})] \\
\hat{c}_{33} &= -(\alpha^4 D_{11} + \beta^4 D_{22} + 2\alpha^2 \beta^2 (D_{12} + 2D_{66})) - \ell^2[\alpha^6 D_{11} + \beta^6 D_{22} + \alpha^4 \beta^2 \\
&\quad (D_{11} + 2D_{12} + 4D_{66}) + \alpha^2 \beta^4 (D_{22} + 2D_{12} + 4D_{66})]
\end{aligned} \tag{21}$$

$$\begin{aligned}
\hat{m}_{11} &= \hat{m}_{22} = I_0 \\
\hat{m}_{13} &= -I_1 \alpha \\
\hat{m}_{23} &= -I_1 \beta \\
\hat{m}_{33} &= I_0 + I_2 (\alpha^2 + \beta^2) \\
\hat{s}_{33} &= (\alpha^2 \hat{N}_{xx} + \beta^2 \hat{N}_{yy})
\end{aligned} \tag{22}$$

114 It is important to point out that, the solution for cross ply laminated
 115 with SS-1 boundary conditions is valid only if:

$$A_{16} = A_{26} = B_{16} = B_{26} = D_{16} = D_{26} = 0 \quad (23)$$

116 *2.2.2. Antisymmetric Angle-Ply Laminates*

117 The Navier displacement field for this case, is assumed to be:

$$\begin{aligned} u_0(x, y) &= \sum_{n=1}^{\infty} \sum_{m=1}^{\infty} U_{mn} \sin \alpha x \cos \beta y \\ v_0(x, y) &= \sum_{n=1}^{\infty} \sum_{m=1}^{\infty} V_{mn} \cos \alpha x \sin \beta y \\ w_0(x, y) &= \sum_{n=1}^{\infty} \sum_{m=1}^{\infty} W_{mn} \sin \alpha x \sin \beta y \end{aligned} \quad (24)$$

118 which satisfies the SS-2 boundary conditions:

$$\begin{aligned} u_0(0, y, t) = 0, u_0(a, y, t) = 0, v_0(x, 0, t) = 0, v_0(x, b, t) = 0 \\ w_0(x, 0, t) = 0, w_0(x, b, t) = 0, w_0(0, y, t) = 0, w_0(a, y, t) = 0 \\ \frac{\partial w_0}{\partial x} \Big|_{(x,0,t)} = 0, \frac{\partial w_0}{\partial x} \Big|_{(x,b,t)} = 0, \frac{\partial w_0}{\partial y} \Big|_{(0,y,t)} = 0, \frac{\partial w_0}{\partial y} \Big|_{(a,y,t)} = 0, \end{aligned} \quad (25)$$

119 where α and β are already defined in the previous subsection.

120 In this case, the coefficient to be employed in Eq. (15), are the following:

$$\begin{aligned}
\hat{c}_{11} &= A_{11}\alpha^2 + A_{66}\beta^2 + \ell^2[A_{11}(\alpha^4 + \alpha^2\beta^2) + A_{66}(\beta^4 + \alpha^2\beta^2)] \\
\hat{c}_{12} &= (A_{12} + A_{66})\alpha\beta + \ell^2(A_{12} + A_{66})(\alpha\beta^3 + \alpha^3\beta) \\
\hat{c}_{13} &= -(3B_{16}\alpha^2\beta + B_{26}\beta^3) - \ell^2[3B_{16}(\alpha^4\beta + \alpha^2\beta^3) + B_{26}(\alpha^2\beta^3 + \beta^5)] \\
\hat{c}_{22} &= A_{66}\alpha^2 + A_{22}\beta^2 + \ell^2[A_{66}(\alpha^4 + \alpha^2\beta^2) + A_{22}(\beta^4 + \alpha^2\beta^2)] \\
\hat{c}_{23} &= -(B_{16}\alpha^3 + 3B_{26}\alpha\beta^2) - \ell^2[B_{16}(\alpha^5 + \alpha^3\beta^2) + 3B_{26}(\alpha\beta^4 + \alpha^3\beta^2)] \\
\hat{c}_{33} &= D_{11}\alpha^4 + 2(D_{12} + 2D_{66})\alpha^2\beta^2 + D_{22}\beta^4 + \ell^2[D_{11}(\alpha^6 + \alpha^4\beta^2) + 2(D_{12} + \\
&\quad + 2D_{66})(\alpha^4\beta^2 + \alpha^2\beta^4) + D_{22}(\alpha^2\beta^4 + \beta^6)]
\end{aligned} \tag{26}$$

$$\begin{aligned}
\hat{m}_{11} &= \hat{m}_{22} = I_0 \\
\hat{m}_{33} &= I_0 + I_2(\alpha^2 + \beta^2) \\
\hat{m}_{23} &= \hat{m}_{13} = 0 \\
\hat{s}_{33} &= (\alpha^2\hat{N}_{xx} + \beta^2\hat{N}_{yy})
\end{aligned} \tag{27}$$

121 Finally, the SS-2 boundary conditions exist only if the stiffness:

$$A_{16} = A_{26} = B_{11} = B_{12} = B_{22} = B_{66} = D_{16} = D_{26} = 0 \tag{28}$$

122 3. Results - Stability analysis

123 3.1. Isotropic

124 Firstly, the outcomes for an isotropic single lamina were carried out in
125 order to make the comparison with Papargyri et al. [50] for the case of buck-
126 ling, assuming gradient elastic material behavior. The lamina is assumed to
127 be simply supported, with the same dimensions along the x and y directions

128 ($a = b$), while the properties of the isotropic material are: $E_1 = E_2 = E = 1$
 129 (E_2 is always considered equal to one in the computations and E_1 will vary
 130 for cross- and angle-ply), $\nu = 0.25$ and $G = 0.5E/(1 + \nu)$. The solution
 131 in terms of buckling load, for uniaxial compression in x direction, which ac-
 132 counts for non locality effects, is dimensionless with respect to the classical
 133 solution ($\ell = 0$). Thus, in the graph below the dimensionless buckling load
 134 \bar{N} is plotted as a function of the normalized gradient coefficient $(\ell/a)^2$, where
 135 the dots represent the solution of the Eq. (16), while the solid line is the
 136 computation of the reference equation from Ref. [50], obtained for $n = m = 1$
 137 which correspond to the minimum value for square plates:

$$\bar{N} = \left[1 + 2\pi^2 \left(\frac{\ell}{a} \right)^2 \right] \quad (29)$$

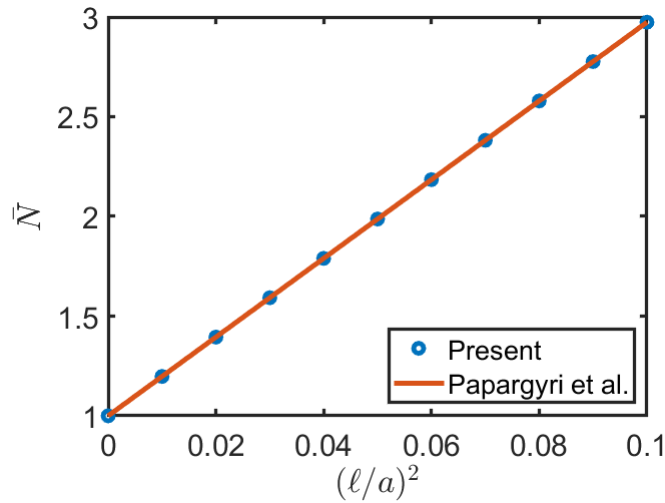


Figure 2: Buckling - comparison with Ref. [50].

138 The Figure 2 shows how in good agreement are the formulations. The
 139 rising trend displays that the critical buckling load grows with non local

140 ratio $(\ell/a)^2$. Note that the minimum buckling load does not always occur for
 141 $m = n = 1$ for rectangular and laminated plate configurations as it will be
 142 discussed in the following. For this reason the minimum buckling load has
 143 been observed to occur within $m, n = 1, 2, 3$ in the present computations.

144 Once Eq. (16) has been verified, it is employed in order to understand
 145 the behavior to changing aspect ratios a/b . The material properties are the
 146 same as the previous case, beside the classical theory $(\ell/a)^2 = 0.00$, two
 147 more values of non local ratios are analyzed $(\ell/a)^2 = 0.05$ and $(\ell/a)^2 = 0.10$,
 148 while the compression is considered for uniaxial and biaxial cases, $k = 0$
 149 and $k = 1$, respectively. It is important to point out that, using the Navier
 150 displacement field only the uniaxial and biaxial cases can be studied, while
 151 not the tangential buckling because the equations cannot work in this case.

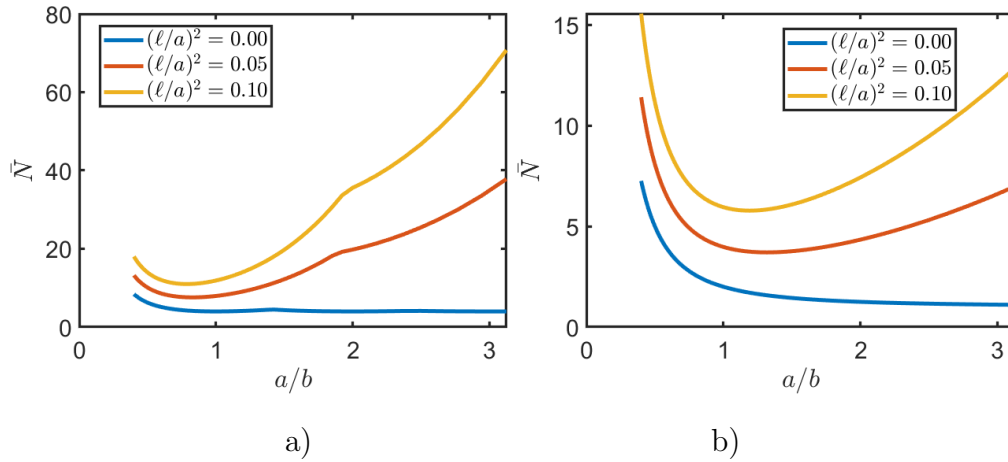


Figure 3: Nondimensionalized buckling load versus plate aspect ratio for isotropic lamina
 - a)Uniaxial compression, b)Biaxial compression

152 From the graph of uniaxial compression, it is possible to see how for
 153 the classical theory, after an initial decreasing of dimensionless buckling load

154 with a/b , the solution has stabilized behavior and quite smooth trend. On
 155 the other hand, if non local effects are involved in the computation, rising
 156 paths are shown since values lower than $a/b = 1$ after the initial decreasing.
 157 Moreover, discontinuities in both trends are displayed for a/b slight lower
 158 than two. From the second graph of Fig. 3, smooth paths are shown for the
 159 three cases and all of them have declining trend in the first phase. Then,
 160 the classical theory presents almost constant \bar{N} since a/b around unity, while
 161 when the lamina is treated with second order theory, it answers with rising
 162 \bar{N} to changing a/b .

163 In both cases, for the whole range of lamina dimensions taken into ac-
 164 count, higher are the values of $(\ell/a)^2$ higher are the critical load magnitudes,
 165 moreover increasing gap between classical and non local theory to rising a/b
 166 are displayed.

167 3.2. Antisymmetric cross-ply

168 Secondly, orthotropic cross-ply plates are studied. For the classical theory
 169 the comparison with Reddy [52] is provided whenever possible, then the
 170 application is extended to the second order theory, presenting outcomes for
 171 $(\ell/a)^2$ equal to 0.05 and 0.10. The ratio E_1/E_2 assumes different magnitudes,
 172 which will be given step by step, while $\nu_{12} = 0.25$, $G_{12} = G_{13} = 0.5E_2$ and
 173 $G_{23} = 0.2E_2$ are the same during the computation. In the first two sections
 174 of the tables 1 and 2, Reddy and present outcomes are reported for the
 175 classical theory, then the application is applied to $(\ell/a)^2$ equal to 0.05 and
 176 0.10. The aspect ratios a/b treated are: 0.5, 1.0 and 1.5, while E_1/E_2 ratio
 177 assumes magnitudes equal to 5, 10, 20, 25 and 40, for $0/90/0/90 = (0/90)_2$
 178 laminate layout. Buckling loads have been reported in dimensionless form as

		E_1/E_2				
a/b		5	10	20	25	40
Reddy [52]	0.5	4.705	4.157	3.828	3.757	3.647
	1	2.643	2.189	1.923	1.866	1.778
	1.5	2.955	2.487	2.211	2.152	2.061
$(\ell/a)^2 = 0.00$	0.5	4.705	4.157	3.828	3.757	3.647
	1	2.643	2.189	1.923	1.866	1.778
	1.5	2.955	2.487	2.211	2.152	2.061
$(\ell/a)^2 = 0.05$	0.5	7.667	6.778	6.234	6.115	5.927
	1	5.422	4.546	3.994	3.868	3.661
	1.5	8.952	7.769	6.968	6.772	6.441
$(\ell/a)^2 = 0.10$	0.5	10.600	9.374	8.623	4.232	8.199
	1	8.131	6.830	6.0138	2.281	5.516
	1.5	14.500	12.617	11.340	3.340	10.486

Table 1: Uniaxial buckling loads ($k = 0$) for $(0/90)_2$ laminate configuration

179 it follows: $\bar{N} = N_{cr}[b^2/(\pi^2 D_{22})]$, considering as maximum order of expansion
180 $m, n = 1, 2, 3$ because the critical buckling load was sought. Table 1 is
181 referred to uniform uniaxial compression ($k = 0$), instead table 2 to biaxial
182 one ($k = 1$).

183 In both Tab. 1 and 2 it is possible to see how results match accurately
184 in the classic application, whereas as it was expected an increasing of the
185 magnitude of the buckling loads is shown for the second order gradient theory.
186 Moreover, it is complicated to make a comparison in terms of variable E_1/E_2
187 and a/b parameter, due to the fluctuating trends within the same theory,

		E_1/E_2				
	a/b	5	10	20	25	40
Reddy [52]	0.5	3.764	3.325	3.062	3.005	2.917
	1	1.322	1.095	0.962	0.933	0.889
	1.5	1.009	0.860	0.773	0.754	0.725
$(\ell/a)^2 = 0.00$	0.5	3.764	3.325	3.062	3.005	2.917
	1	1.322	1.095	0.962	0.933	0.889
	1.5	1.009	0.860	0.773	0.754	0.725
$(\ell/a)^2 = 0.05$	0.5	6.134	5.423	4.987	4.892	4.742
	1	2.711	2.273	1.997	1.934	1.830
	1.5	2.754	2.390	2.144	2.084	1.982
$(\ell/a)^2 = 0.10$	0.5	8.480	7.499	6.899	6.767	6.559
	1	4.065	3.415	3.007	2.913	2.758
	1.5	4.462	3.882	3.489	3.393	3.226

Table 2: Biaxial buckling loads ($k = 1$) for $(0/90)_2$ laminate configuration

188 especially for $k = 0$. Thus, in order to draw conclusions it is needed to
 189 represent outcomes in graphical form, wherein material properties chosen for
 190 the analysis are: $E_1/E_2 = 25$ and $E_1/E_2 = 40$. The laminate configurations
 191 studied are: $(0/90)$, $(0/90)_2$ and $(0/90)_4$ for the uniform uniaxial compression
 192 ($k = 0$), while for the biaxial case $(0/90)$, $(0/90)_2$ and $(0/90)_3$ are taken into
 193 account. The dimensionless expression used, is again: $\bar{N} = N_{cr}[b^2/(\pi^2 D_{22})]$,
 194 with a maximum expansion order of $m, n = 1, 2, 3$.

195 In Fig. 4 and 5, it is possible to see how the classical theory displays the
 196 lower critical loads for every laminate configuration, material and uniform
 197 compression type. It shows also discontinuities for the uniaxial compression,
 198 instead smooth trends for biaxial one, because the buckling load is not given
 199 by $m = n = 1$ for rectangular plates as discussed in classical references [52].
 200 Moreover, for both classical and second gradient order theories, an initial
 201 reduction of the buckling load is shown, in the first case it is followed by a
 202 quite constant path, while for the second case it is visible the growing mag-
 203 nitude with increasing value of aspect ratio, where slope expands with non
 204 local ratios. Laminae made by the same sequence of layers, but accounting
 205 for different materials are studied and it comes out that if $E_1/E_2 = 25$ is
 206 considered as property of the material, an higher magnitude of buckling load
 207 is displaced compared to $E_1/E_2 = 40$ case. From the comparison among dif-
 208 ferent layouts for both uniaxial and biaxial compression, it comes out that,
 209 to parity of materials and plate thickness, the lower critical load belongs to
 210 $(0/90)$ configuration, while its value grows as more layers are added to the
 211 plate.

E_1/E_2		10	25	40
(45/ - 45)	Reddy [52]	9.066	15.476	21.709
	$(\ell/a)^2 = 0.00$	9.066	15.476	21.709
	$(\ell/a)^2 = 0.05$	18.015	30.750	43.135
	$(\ell/a)^2 = 0.10$	26.963	46.024	64.561
(45/ - 45) ₄	Reddy [52]	17.637	41.163	64.683
	$(\ell/a)^2 = 0.00$	17.637	41.163	64.683
	$(\ell/a)^2 = 0.05$	35.043	81.789	128.522
	$(\ell/a)^2 = 0.10$	52.450	122.415	192.362

Table 3: Uniaxial buckling loads for (45/ - 45) and (45/ - 45)₄ laminate configurations

212 *3.3. Antisymmetric angle-ply*

213 Finally, in this section orthotropic angle-ply laminates are studied. As in
214 the previous case in tables 3 and 4, the first two sections are referred to the
215 comparison with Reddy of the classical theory [52], then it is extended to
216 the second-order strain gradient theory. All the parameters employed can be
217 picked from the previous paragraph, except the laminates taken into account
218 which are: (45/ - 45) and (45/ - 45)₄, while the E_1/E_2 ratios are specified in
219 the tables. Both uniform uniaxial ($k = 0$) and biaxial ($k = 1$) compression
220 of the square plate, along x , and x and y are carried out, using the following
221 dimensionless expression: $\bar{N} = N_{cr}[b^2/(h^3 E_2)]$.

222 From both Tab 3 and 4, the comparison for the classical theory leads to
223 good confidence in the method also for orthotropic antisymmetric angle-ply
224 laminates. Moreover, as in the earlier case it is possible to see an increasing in
225 magnitude of the dimensionless buckling load to rising $(\ell/a)^2$. Consequently,

E_1/E_2		10	25	40
(45/ - 45)	Reddy [52]	4.533	7.738	10.854
	$(\ell/a)^2 = 0.00$	4.533	7.738	10.854
	$(\ell/a)^2 = 0.05$	9.007	15.375	21.567
	$(\ell/a)^2 = 0.10$	13.481	23.012	32.280
(45/ - 45) ₄	Reddy [52]	8.818	20.581	32.341
	$(\ell/a)^2 = 0.00$	8.818	20.581	32.341
	$(\ell/a)^2 = 0.05$	17.522	40.895	64.261
	$(\ell/a)^2 = 0.10$	26.225	61.208	96.181

Table 4: Biaxial buckling loads for (45/ - 45) and (45/ - 45)₄ laminate configurations

226 as it follows, a deeper study in order to catch the trend of $(-45/45)_i$, (with
227 $i = 1, 2, 3, 4$) laminate configurations is carried out, enlarging the range of
228 a/b up to five and considering E_1/E_2 equal to 25 and 40, in both $k = 0$ and
229 $k = 1$ conditions.

230 As for the cross-ply laminates, the figures 6 and 7 show higher values of
231 dimensionless buckling load for values of non local ratio equal to 0.10. Also,
232 when $k = 0$ the classical theory displays flat trends, differently from the
233 second-order strain gradient theory which presents rough tendency, instead if
234 $k = 1$ they are always smooth. The behavior in case of $(\ell/a)^2 = 0$ presents an
235 original decreasing followed by a stable trend, viceversa if $(\ell/a)^2$ is non zero
236 the consecutive part grows up to very high values. In addition, comparing
237 the different behavior of the plates it is possible to assert that to parity of
238 material, the six-layered plate shows much higher critical load for every a/b ,
239 and comparing the two-, four- and six-layered laminate in $k = 0$ and $k = 1$

240 it is possible to see that for uniaxial case the structures buckles for much
241 higher values.

242 4. Results - Dynamic analysis

243 4.1. Isotropic

244 Accordingly to what previously done for the stability analysis, also for
245 the free vibration analysis the first step is to compare the present solution
246 to the Papargyri et al. [50], which is expressed by Eq.(30) for isotropic
247 materials. The material properties, of the square plate ($a = b$), are the
248 following: $E_1/E_2 = 1$, $\nu = 0.25$ and $G = 0.5E/(1 + \nu)$. The dimensionless
249 frequency $\bar{\omega}$

$$\bar{\omega} = \sqrt{1 + 2\pi^2 \left(\frac{\ell}{a}\right)^2} \quad (30)$$

250 has been plotted for changing dimensionless $(\ell/a)^2$, for $n = m = 1$. In
251 Fig. 8 it is possible to see how outcomes match accurately, where the dots
252 represent the solution of the Eq. (17), and the solid line is referred to the
253 computation of Eq. (30), showing a rising parabolic behavior for the range
254 of $(\ell/a)^2$ within 0 and 0.1. Thus, the study has been extended in order to
255 understand the behavior for different plate geometries. In fact, outcomes are
256 plotted in Fig. 9 considering an isotropic lamina, for non local ratios equal
257 to 0, 0.05 and 0.10.

258 It is possible to see an increasing of the dimensionless frequency magni-
259 tude with $(\ell/a)^2$, for the whole path, showing higher gaps among theories
260 as a/b rises. Moreover, the initial decreasing is followed by a stable trend

261 for the classical theory ($(\ell/a)^2 = 0$) and by a rising one for the second-order
262 strain gradient theory.

263 4.2. Antisymmetric cross-ply

264 Then, analysis continues facing to antisymmetric cross-ply laminates.
265 Whenever it has been possible, comparisons with Reddy [52] are carried
266 out for $(\ell/a)^2 = 0$, then results are extended to second-order strain gradient
267 theory. In table 5, dimensionless frequencies of square antisymmetric cross-
268 ply laminates (layouts: $(0/90)$, $(0/90)_2$ and $(0/90)_4$) are carried out imposing
269 $m, n = 1, 2, 3$. The comparison with Reddy [52] is provided in its first two
270 sections for the classical theory, then the theory has been developed also for
271 $(\ell/a)^2$ equal to 0.05 and 0.10. The material properties are given: E_1/E_2 equal
272 to 10 and 20, $\nu_{12} = 0.25$, $G_{12} = G_{13} = 0.5E_2$ and $G_{23} = 0.2E_2$. The frequency
273 is dimensionless with respect to the following formula: $\bar{\omega} = \omega b^2 / \pi^2 \sqrt{\rho h / D_{22}}$.

274 In Tab. 5 is it possible to see how results are in good agreement for what
275 concerns the classical theory. Moreover, $\bar{\omega}$ increases with the number of layers
276 in the laminate accounting for the same total thickness, for every mode and
277 value of non local ratio. Thus, graphic results are drawn, for $(0/90)$, $(0/90)_2$
278 and $(0/90)_4$ configurations, employing $m, n = 1, 2, 3$. Fundamental frequency
279 is carried out with respect to the aspect ratio a/b , for magnitude of non local
280 ratio $(\ell/a)^2$ equal to 0.00, 0.05 and 0.10. Materials selected are given by
281 E_1/E_2 equal to 25 and 40, $\nu_{12} = 0.25$, $G_{12} = G_{13} = 0.5E_2$.

282 In Fig. 10, for the classical theory case, it is possible to see a reducing
283 magnitude of dimensionless fundamental frequency which stabilizes for val-
284 ues of a/b between 1 and 2, for every geometrical configuration and material
285 property. This is similar in the initial stage for second-order strain gradient

E_1/E_2			10			20		
	m	n	(0/90)	(0/90) ₂	(0/90) ₄	(0/90)	(0/90) ₂	(0/90) ₄
Reddy [52]	1	1	1.183	1.479	1.545	0.990	1.386	1.469
	1	2	3.174	4.077	4.274	2.719	3.913	4.158
	1	3	6.666	8.698	9.136	5.789	8.456	8.998
	2	1	3.174	4.077	4.274	2.719	3.913	4.158
	2	2	4.733	5.918	6.179	3.959	5.547	5.877
	2	3	7.927	10.034	10.494	6.702	9.507	10.088
	3	1	6.666	8.698	9.136	5.789	8.456	8.998
	3	2	7.927	10.034	10.494	6.193	9.507	10.088
	3	3	10.650	13.317	13.904	8.908	12.481	13.224
$(\ell/a)^2 = 0.00$	1	1	1.183	1.480	1.545	0.990	1.387	1.469
	1	2	3.174	4.078	4.274	2.719	3.913	4.158
	1	3	6.666	8.698	9.136	5.789	8.455	8.998
	2	1	3.174	4.078	4.274	2.719	3.913	4.158
	2	2	4.733	5.918	6.179	3.959	5.547	5.877
	2	3	7.927	10.033	10.494	6.702	9.507	10.088
	3	1	6.666	8.698	9.136	5.789	8.455	8.998
	3	2	7.927	10.033	10.494	6.702	9.507	10.088
	3	3	10.650	13.317	13.903	8.908	12.481	13.224
$(\ell/a)^2 = 0.05$	1	1	1.888	2.132	2.189	1.625	1.999	2.082
	1	2	7.135	7.851	8.020	6.267	7.517	7.798
	1	3	19.151	21.790	22.401	16.758	21.088	22.038
	2	1	6.159	7.642	7.969	5.338	7.335	7.754
	2	2	12.522	13.594	13.849	11.354	12.848	13.195
	2	3	27.962	28.731	28.920	26.420	27.595	27.882
	3	1	16.487	21.238	22.268	14.343	20.638	21.931
	3	2	23.449	27.703	28.668	20.521	26.311	27.569
	3	3	39.910	43.249	44.044	36.312	40.902	41.971
$(\ell/a)^2 = 0.10$	1	1	2.333	2.614	2.679	2.023	2.452	2.548
	1	2	9.435	10.295	10.498	8.335	9.862	10.208
	1	3	26.104	29.530	30.326	22.893	28.582	29.835
	2	1	8.058	9.998	10.426	6.985	9.597	10.145
	2	2	16.795	18.229	18.570	15.235	17.230	17.694
	2	3	38.201	39.241	39.497	36.113	37.695	38.080
	3	1	22.313	28.742	30.136	19.411	27.930	29.680
	3	2	32.025	37.834	39.152	28.026	35.933	37.652
	3	3	54.997	59.596	60.691	50.041	56.362	57.835

Table 5: Dimensionless frequencies $\bar{\omega}$ of antisymmetric cross-ply laminates

E_1/E_2	25		40	
	(-45/45)	(-45/45) ₄	(45/ - 45)	(45/ - 45) ₃
Reddy [52]	12,357	20,154	14,636	24,825
$(\ell/a)^2 = 0.00$	12,358	20,154	14,636	24,825
$(\ell/a)^2 = 0.05$	17,419	28,409	20,631	34,994
$(\ell/a)^2 = 0.10$	21,311	34,756	25,241	42,812

Table 6: Dimensionless frequencies $\bar{\omega}$ of antisymmetric angle-ply laminates

theory, even if for the whole study they show greater magnitude, while they display an increasing trend for values around 1.2 onwards. It is also possible to say that, $\bar{\omega}$ has greater magnitude as the number of the layer of the plate increases accounting for the same thickness and for lower E_1/E_2 ratios. Finally, as previously demonstrated dimensionless fundamental frequency increases as $(\ell/a)^2$ rises.

4.3. Antisymmetric angle-ply

The last step of the present paper is focused on the analysis of the antisymmetric angle-ply laminates in terms of dimensionless frequency. Firstly, three different layouts of squared plate are considered: (-45/45), (-45/45)₄, (45/ - 45) and (45/ - 45)₄. The material properties for the first two columns are: $E_1/E_2 = 25$, $\nu_{12} = 0.25$, $G_{12} = G_{13} = 0.5E_2$ and for the last two $E_1/E_2 = 40$, $\nu_{12} = 0.25$, $G_{12} = G_{13} = 0.6E_2$. The frequency is dimensionless as following: $\bar{\omega} = \omega a^2 / h \sqrt{\rho/E_2}$ and $n = m = 1$ is considered.

In the first two rows of Tab. 6, the comparison with Reddy [52] for the classical theory was made showing perfect agreement. The third and fourth rows display the extension to the second-order strain gradient theory, for

303 which outcomes have a rising trend with $(\ell/a)^2$ for each case.

304 Finally, trends by changing a/b (increased from three to five) are drawn in
305 Fig. 11, for $m, n = 1, 2, 3$, in terms of dimensionless fundamental frequency:
306 $\bar{\omega} = \omega b^2 / \pi^2 \sqrt{\rho h / D_{22}}$. Material properties chosen as E_1/E_2 equal to 25 and
307 40, $\nu_{12} = 0.25$, $G_{12} = G_{13} = 0.5E_2$. The plates configurations that are
308 studied are: $(-45/45)$, $(-45/45)_2$ and $(-45/45)_3$.

309 In the graph 11 trends similar to the cross-ply case are shown, on the other
310 hand much higher magnitudes of dimensionless fundamental frequencies are
311 reached in the present case. Decreasing in the early phase and then constant
312 behavior is shown for the classical theory ($(\ell/a)^2 = 0.00$), on the contrary a
313 growing behavior by changing a/b if non local effects are taken into account
314 is observed for $(\ell/a)^2 = 0.05$ and $(\ell/a)^2 = 0.10$. It is also displayed as the
315 magnitude of $\bar{\omega}$ grows for a major number of layers in the plate configuration
316 to parity of thickness. The last observation regards the materials, in fact it
317 is clear as $\bar{\omega}$ illustrates a slight more significant impact if the ratio E_1/E_2 is
318 equal to 25.

319 5. Conclusion

320 In the present paper, the stability and dynamic analysis of simply sup-
321 ported nano plates are examined, applying the Kirchhoff theory and Navier
322 solution method. An assortment of plate layouts, materials and geometries
323 are involved, comparisons for the classical case wherever it was possible are
324 provided, then outcomes are extended to the second-order strain gradient
325 theory, thus taking into account nonlocal effects.

326 Firstly, making an analogy between laminates, for both cross- and angle-

ply, in uniaxial and biaxial cases, it is clear that it is possible to exploit the higher resistance of orthotropic angle-ply plates against buckling issues compared to the cross-ply plates. Moreover, for what concerns the dimensions of the laminate in order to avoid early collapse it is needed to avoid a/b close to one, when higher order theory is employed to catch the nano plates behavior. Also, in the same material and geometrical conditions, it is preferable to use plates made by more layers to parity of plate thickness.

Finally, the procedure applied for the dynamic analysis shows non linear trends for cross- and angle-ply laminates by changing plate aspect ratios. Moreover, in this case it is also shown the much higher magnitude in terms of dimensionless fundamental frequency if angle-ply plates are employed. Also, for a defined plate thickness, the application of a greater number of layers, as well as the use of material with lower ratio E_1/E_2 induces to more considerable values of dimensionless frequency of the structure.

In conclusion, from this study comes out that the performance of the second-order strain gradient theory is different from the classical one on by far, and the gap increases with plate aspect ratio and with non local ratio, thus nano plates need to be analyzed by considering non local effects.

Appendix A. Appendix

Differential operators of the Hamilton's Principle are explicitly given below, where f indicates the generic derivative operator to be applied for the partial derivation (for instance $f_{,x} = \frac{\partial}{\partial x}$):

$$\mathcal{T}_{11} = A_{11}f_{,x} + A_{16}f_{,y} - \ell^2 \left[A_{11} \left(f_{,xxx} + f_{,xyy} \right) + A_{16} \left(f_{,xyy} + f_{,yyy} \right) \right] \quad (\text{A.1})$$

$$\mathcal{T}_{12} = A_{12}f_{,y} + A_{16}f_{,x} - \ell^2 \left[A_{12} \left(f_{,yyy} + f_{,xxy} \right) + A_{16} \left(f_{,xyy} + f_{,xxx} \right) \right] \quad (\text{A.2})$$

$$\begin{aligned} \mathcal{T}_{13} = & - \left(B_{11}f_{,xx} + B_{12}f_{,yy} + 2B_{16}f_{,xy} \right) + \ell^2 \left[B_{11} \left(f_{,xxxx} + f_{,xxyy} \right) + \right. \\ & \left. + B_{12} \left(f_{,xxyy} + f_{,yyyy} \right) + 2B_{16} \left(f_{,xxyy} + f_{,xyyy} \right) \right] \end{aligned} \quad (\text{A.3})$$

$$\mathcal{T}_{21} = A_{16}f_{,x} + A_{66}f_{,y} - \ell^2 \left[A_{16} \left(f_{,xxx} + f_{,xyy} \right) + A_{66} \left(f_{,xxy} + f_{,yyy} \right) \right] = \mathcal{T}_{31} \quad (\text{A.4})$$

$$\mathcal{T}_{22} = A_{26}f_{,y} + A_{66}f_{,x} - \ell^2 \left[A_{26} \left(f_{,yyy} + f_{,xxy} \right) + A_{66} \left(f_{,xyy} + f_{,xxx} \right) \right] = \mathcal{T}_{32} \quad (\text{A.5})$$

$$\begin{aligned} \mathcal{T}_{23} = & - \left(B_{16}f_{,xx} + B_{26}f_{,yy} + 2B_{66}f_{,xy} \right) + \ell^2 \left[B_{16} \left(f_{,xxxx} + f_{,xxyy} \right) + \right. \\ & \left. + B_{26} \left(f_{,xxyy} + f_{,yyyy} \right) + 2B_{66} \left(f_{,xxyy} + f_{,xyyy} \right) \right] = \mathcal{T}_{33} \end{aligned} \quad (\text{A.6})$$

$$\mathcal{T}_{31} = A_{16}f_{,x} + A_{66}f_{,y} - \ell^2 \left[A_{16} \left(f_{,xxx} + f_{,xyy} \right) + A_{66} \left(f_{,xxy} + f_{,yyy} \right) \right] \quad (\text{A.7})$$

$$\mathcal{T}_{32} = A_{26}f_{,y} + A_{66}f_{,x} - \ell^2 \left[A_{26} \left(f_{,yyy} + f_{,xxy} \right) + A_{66} \left(f_{,xyy} + f_{,xxx} \right) \right] \quad (\text{A.8})$$

$$\begin{aligned} \mathcal{T}_{33} = & -\left(B_{16}f_{,xx} + B_{26}f_{,yy} + 2B_{66}f_{,xy}\right) + \ell^2 \left[B_{16} \left(f_{,xxxx} + f_{,xxyy} \right) + \right. \\ & \left. + B_{26} \left(f_{,xxyy} + f_{,yyyy} \right) + 2B_{66} \left(f_{,xxyy} + f_{,xyyy} \right) \right] \end{aligned} \quad (\text{A.9})$$

$$\mathcal{T}_{41} = A_{12}f_{,x} + A_{26}f_{,y} - \ell^2 \left[A_{12} \left(f_{,xxx} + f_{,xyy} \right) + A_{26} \left(f_{,xxy} + f_{,yyy} \right) \right] \quad (\text{A.10})$$

$$\mathcal{T}_{42} = A_{22}f_{,y} + A_{26}f_{,x} - \ell^2 \left[A_{22} \left(f_{,yyy} + f_{,xxy} \right) + A_{26} \left(f_{,xxy} + f_{,yyy} \right) \right] \quad (\text{A.11})$$

$$\begin{aligned} \mathcal{T}_{43} = & -\left(B_{12}f_{,xx} + B_{22}f_{,yy} + 2B_{26}f_{,xy}\right) + \ell^2 \left[B_{12} \left(f_{,xxxx} + f_{,xxyy} \right) + \right. \\ & \left. + B_{22} \left(f_{,xxyy} + f_{,yyyy} \right) + 2B_{26} \left(f_{,xyyy} + f_{,xxyy} \right) \right] \end{aligned} \quad (\text{A.12})$$

$$\mathcal{T}_{51} = -\left(B_{11}f_{,x} + B_{16}f_{,y}\right) + \ell^2 \left[B_{11} \left(f_{,xxx} + f_{,xyy} \right) + B_{16} \left(f_{,xxy} + f_{,yyy} \right) \right] \quad (\text{A.13})$$

$$\mathcal{T}_{52} = -\left(B_{12}f_{,y} + B_{16}f_{,x}\right) + \ell^2 \left[B_{12} \left(f_{,yyy} + f_{,xxy} \right) + B_{16} \left(f_{,xxy} + f_{,xxx} \right) \right] \quad (\text{A.14})$$

$$\begin{aligned} \mathcal{T}_{53} = & D_{11}f_{,xx} + D_{12}f_{,yy} + 2D_{16}f_{,xy} - \ell^2 \left[D_{11} \left(f_{,xxxx} + f_{,xxyy} \right) + \right. \\ & \left. + D_{12} \left(f_{,xxyy} + f_{,yyyy} \right) + 2D_{16} \left(f_{,xyyy} + f_{,xxyy} \right) \right] \end{aligned} \quad (\text{A.15})$$

$$\mathcal{T}_{61} = -\left(B_{12}f_{,x} + B_{26}f_{,y}\right) + \ell^2 \left[B_{12} \left(f_{,xxx} + f_{,xyy} \right) + B_{26} \left(f_{,xxy} + f_{,yyy} \right) \right] \quad (\text{A.16})$$

$$\mathcal{T}_{62} = -\left(B_{22}f_{,y} + B_{26}f_{,x}\right) + \ell^2 \left[B_{22} \left(f_{,yyy} + f_{,xxy} \right) + B_{26} \left(f_{,xyy} + f_{,xxx} \right) \right] \quad (\text{A.17})$$

$$\begin{aligned} \mathcal{T}_{63} = & D_{12}f_{,xx} + D_{22}f_{,yy} + 2D_{26}f_{,xy} - \ell^2 \left[D_{12} \left(f_{,xxxx} + f_{,xxyy} \right) \right. \\ & \left. + D_{22} \left(f_{,xxyy} + f_{,yyyy} \right) + 2D_{26} \left(f_{,xyyy} + f_{,xxxy} \right) \right] \end{aligned} \quad (\text{A.18})$$

$$\begin{aligned} \mathcal{T}_{71} = & 2 \left[- \left(B_{16}f_{,x} + B_{66}f_{,y} \right) + \ell^2 \left(B_{16} \left(f_{,xxx} + f_{,xyy} \right) \right. \right. \\ & \left. \left. + B_{66} \left(f_{,xxy} + f_{,yyy} \right) \right) \right] \end{aligned} \quad (\text{A.19})$$

$$\begin{aligned} \mathcal{T}_{72} = & 2 \left[- \left(B_{26}f_{,y} + B_{66}f_{,x} \right) + \ell^2 \left(B_{26} \left(f_{,yyy} + f_{,xxy} \right) \right. \right. \\ & \left. \left. + B_{66} \left(f_{,xyy} + f_{,xxx} \right) \right) \right] \end{aligned} \quad (\text{A.20})$$

$$\begin{aligned} \mathcal{T}_{73} = & 2 \left[D_{16}f_{,xx} + D_{26}f_{,yy} + 2D_{66}f_{,xy} - \ell^2 \left(D_{16} \left(f_{,xxxx} + f_{,xxyy} \right) \right. \right. \\ & \left. \left. + D_{26} \left(f_{,xxyy} + f_{,yyyy} \right) + 2D_{66} \left(f_{,xyyy} + f_{,xxxy} \right) \right) \right] \end{aligned} \quad (\text{A.21})$$

349 **References**

- 350 [1] C. Li, E. T. Thostenson, T.-W. Chou, Sensors and actuators based on
351 carbon nanotubes and their composites: a review, *Composites science*
352 *and technology* 68 (2008) 1227–1249.
- 353 [2] K. Ekinici, M. Roukes, Nanoelectromechanical systems, *Review of sci-*
354 *entific instruments* 76 (2005) 061101.
- 355 [3] M. Mohammadimehr, H. M. Hooyeh, H. Afshari, M. R. Salarkia, Free
356 vibration analysis of double-bonded isotropic piezoelectric timoshenko
357 microbeam based on strain gradient and surface stress elasticity theories
358 under initial stress using differential quadrature method, *Mechanics of*
359 *Advanced Materials and Structures* 24 (2017) 287–303.
- 360 [4] R. Barretta, L. Feo, R. Luciano, F. M. de Sciarra, A gradient erin-
361 gen model for functionally graded nanorods, *Composite Structures* 131
362 (2015) 1124–1131.
- 363 [5] B. Bhushan, Nanotribology and nanomechanics of mems/nems and
364 biomems/bionems materials and devices, *Microelectronic Engineering*
365 84 (2007) 387–412.
- 366 [6] D. Berman, J. Krim, Surface science, mems and nems: Progress and
367 opportunities for surface science research performed on, or by, microde-
368 vices, *Progress in Surface Science* 88 (2013) 171–211.
- 369 [7] V. S. Saji, H. C. Choe, K. W. Yeung, Nanotechnology in biomedical
370 applications: a review, *International Journal of Nano and Biomaterials*
371 3 (2010) 119–139.

- 372 [8] P. Sharma, S. Ganti, N. Bhate, Effect of surfaces on the size-dependent
373 elastic state of nano-inhomogeneities, *Applied Physics Letters* 82 (2003)
374 535–537.
- 375 [9] B. Wang, S. Zhou, J. Zhao, X. Chen, A size-dependent kirchhoff micro-
376 plate model based on strain gradient elasticity theory, *European Journal*
377 *of Mechanics - A/Solids* 30 (2011) 517 – 524.
- 378 [10] A. Li, S. Zhou, S. Zhou, B. Wang, A size-dependent model for bi-
379 layered kirchhoff micro-plate based on strain gradient elasticity theory,
380 *Composite Structures* 113 (2014) 272 – 280.
- 381 [11] B. Akgöz, Ö. Civalek, A microstructure-dependent sinusoidal plate
382 model based on the strain gradient elasticity theory, *Acta Mechanica*
383 226 (2015) 2277–2294.
- 384 [12] M. R. Barati, N. M. Faleh, A. M. Zenkour, Dynamic response of
385 nanobeams subjected to moving nanoparticles and hygro-thermal en-
386 vironments based on nonlocal strain gradient theory, *Mechanics of Ad-*
387 *vanced Materials and Structures* 0 (2018) 1–9.
- 388 [13] A. W. McFarland, J. S. Colton, Role of material microstructure in plate
389 stiffness with relevance to microcantilever sensors, *Journal of Microme-*
390 *chanics and Microengineering* 15 (2005) 1060.
- 391 [14] D. C. Lam, F. Yang, A. Chong, J. Wang, P. Tong, Experiments and
392 theory in strain gradient elasticity, *Journal of the Mechanics and Physics*
393 *of Solids* 51 (2003) 1477–1508.

- 394 [15] J. S. Stölken, A. Evans, A microbend test method for measuring the
395 plasticity length scale, *Acta Materialia* 46 (1998) 5109–5115.
- 396 [16] J. H. Lii, N. L. Allinger, Molecular mechanics. the mm3 force field
397 for hydrocarbons. 3. the van der waals' potentials and crystal data for
398 aliphatic and aromatic hydrocarbons, *Journal of the American Chemical*
399 *Society* 111 (1989) 8576–8582.
- 400 [17] N. L. Allinger, Conformational analysis. 130. mm2. a hydrocarbon force
401 field utilizing v1 and v2 torsional terms, *Journal of the American Chem-*
402 *ical Society* 99 (1977) 8127–8134.
- 403 [18] J. Tersoff, New empirical approach for the structure and energy of
404 covalent systems, *Physical Review B* 37 (1988) 6991.
- 405 [19] D. W. Brenner, Empirical potential for hydrocarbons for use in simu-
406 lating the chemical vapor deposition of diamond films, *Physical review*
407 *B* 42 (1990) 9458.
- 408 [20] A. Ashoori, M. J. Mahmoodi, A nonlinear thick plate formulation based
409 on the modified strain gradient theory, *Mechanics of Advanced Materials*
410 *and Structures* 25 (2018) 813–819.
- 411 [21] B. Babu, B. Patel, A new computationally efficient finite element for-
412 mulation for nanoplates using second-order strain gradient kirchhoff's
413 plate theory, *Composites Part B: Engineering* 168 (2019) 302–311.
- 414 [22] M. Hosseini, A. Jamalpoor, A. Fath, Surface effect on the biaxial buck-
415 ling and free vibration of fgm nanoplate embedded in visco-pasternak

- 416 standard linear solid-type of foundation, *Meccanica* 52 (2017) 1381–
417 1396.
- 418 [23] B. Akgöz, Ö. Civalek, Bending analysis of embedded carbon nanotubes
419 resting on an elastic foundation using strain gradient theory, *Acta As-*
420 *tronautica* 119 (2016) 1–12.
- 421 [24] Ç. Demir, Ö. Civalek, On the analysis of microbeams, *International*
422 *Journal of Engineering Science* 121 (2017) 14–33.
- 423 [25] B. Akgöz, Ö. Civalek, Bending analysis of fg microbeams resting on win-
424 kler elastic foundation via strain gradient elasticity, *Composite Struc-*
425 *tures* 134 (2015) 294–301.
- 426 [26] A. C. Eringen, Nonlocal polar elastic continua, *International journal of*
427 *engineering science* 10 (1972) 1–16.
- 428 [27] K. Lazopoulos, On bending of strain gradient elastic micro-plates, *Me-*
429 *chanics Research Communications* 36 (2009) 777 – 783.
- 430 [28] A. A. Movassagh, M. Mahmoodi, A micro-scale modeling of kirchhoff
431 plate based on modified strain-gradient elasticity theory, *European Jour-*
432 *nal of Mechanics - A/Solids* 40 (2013) 50 – 59.
- 433 [29] M. Mirsalehi, M. Azhari, H. Amoushahi, Buckling and free vibration of
434 the fgm thin micro-plate based on the modified strain gradient theory
435 and the spline finite strip method, *European Journal of Mechanics -*
436 *A/Solids* 61 (2017) 1 – 13.

- 437 [30] C. Li, L. Yao, W. Chen, S. Li, Comments on nonlocal effects in nano-
438 cantilever beams, *International Journal of Engineering Science* 87 (2015)
439 47–57.
- 440 [31] B. Akgöz, Ö. Civalek, Analysis of micro-sized beams for various bound-
441 ary conditions based on the strain gradient elasticity theory, *Archive of*
442 *Applied Mechanics* 82 (2012) 423–443.
- 443 [32] A. C. Eringen, On differential equations of nonlocal elasticity and solu-
444 tions of screw dislocation and surface waves, *Journal of applied physics*
445 54 (1983) 4703–4710.
- 446 [33] E. C. Aifantis, On the role of gradients in the localization of deformation
447 and fracture, *International Journal of Engineering Science* 30 (1992)
448 1279–1299.
- 449 [34] S. Altan, E. Aifantis, On the structure of the mode iii crack-tip in
450 gradient elasticity, *Scripta Metallurgica et Materialia* 26 (1992) 319–
451 324.
- 452 [35] C. Ru, E. Aifantis, A simple approach to solve boundary-value problems
453 in gradient elasticity, *Acta Mechanica* 101 (1993) 59–68.
- 454 [36] C. S. Chang, J. Gao, Second-gradient constitutive theory for granular
455 material with random packing structure, *International Journal of Solids*
456 *and Structures* 32 (1995) 2279–2293.
- 457 [37] H. Mühlhaus, F. Oka, Dispersion and wave propagation in discrete and
458 continuous models for granular materials, *International Journal of Solids*
459 *and Structures* 33 (1996) 2841–2858.

- 460 [38] F. Yang, A. Chong, D. C. C. Lam, P. Tong, Couple stress based strain
461 gradient theory for elasticity, *International Journal of Solids and Structures* 39 (2002) 2731–2743.
462
- 463 [39] F. Ebrahimi, M. R. Barati, Vibration analysis of biaxially compressed
464 double-layered graphene sheets based on nonlocal strain gradient theory,
465 *Mechanics of Advanced Materials and Structures* 26 (2019) 854–865.
- 466 [40] Y. Li, Z. Cai, S. Shi, Buckling and free vibration of magnetoelastic
467 nanoplate based on nonlocal theory, *Composite Structures* 111 (2014)
468 522 – 529.
- 469 [41] A. Farajpour, M. Danesh, M. Mohammadi, Buckling analysis of variable
470 thickness nanoplates using nonlocal continuum mechanics, *Physica E:
471 Low-dimensional Systems and Nanostructures* 44 (2011) 719 – 727.
- 472 [42] T. Aksencer, M. Aydogdu, Levy type solution method for vibration
473 and buckling of nanoplates using nonlocal elasticity theory, *Physica E:
474 Low-dimensional Systems and Nanostructures* 43 (2011) 954 – 959.
- 475 [43] Z. Yan, L. Y. Jiang, Vibration and buckling analysis of a piezoelectric
476 nanoplate considering surface effects and in-plane constraints, *Proceed-
477 ings of the Royal Society A: Mathematical, Physical and Engineering
478 Sciences* 468 (2012) 3458–3475.
- 479 [44] H. B. Khaniki, S. Hosseini-Hashemi, Dynamic response of biaxially
480 loaded double-layer viscoelastic orthotropic nanoplate system under a
481 moving nanoparticle, *International Journal of Engineering Science* 115
482 (2017) 51 – 72.

- 483 [45] K. Kiani, Small-scale effect on the vibration of thin nanoplates subjected
484 to a moving nanoparticle via nonlocal continuum theory, *Journal of*
485 *Sound and Vibration* 330 (2011) 4896 – 4914.
- 486 [46] R. Kolahchi, H. Hosseini, M. Esmailpour, Differential cubature
487 and quadrature-bolotin methods for dynamic stability of embedded
488 piezoelectric nanoplates based on visco-nonlocal-piezoelasticity theories,
489 *Composite Structures* 157 (2016) 174 – 186.
- 490 [47] A. Assadi, B. Farshi, A. Alinia-Ziazi, Size dependent dynamic analysis
491 of nanoplates, *Journal of Applied Physics* 107 (2010) 124310.
- 492 [48] S. Rajasekaran, H. B. Khaniki, Finite element static and dynamic anal-
493 ysis of axially functionally graded nonuniform small-scale beams based
494 on nonlocal strain gradient theory, *Mechanics of Advanced Materials*
495 *and Structures* 26 (2019) 1245–1259.
- 496 [49] R. Kolahchi, M. S. Zarei, M. H. Hajmohammad, A. N. Oskouei,
497 Visco-nonlocal-refined zigzag theories for dynamic buckling of laminated
498 nanoplates using differential cubature-bolotin methods, *Thin-Walled*
499 *Structures* 113 (2017) 162 – 169.
- 500 [50] S. Papargyri-Beskou, D. E. Beskos, Static, stability and dynamic anal-
501 ysis of gradient elastic flexural kirchhoff plates, *Archive of Applied*
502 *Mechanics* 78 (2008) 625–635.
- 503 [51] F. Cornacchia, N. Fantuzzi, R. Luciano, R. Penna, Solution for cross-
504 and angle-ply laminated kirchhoff nano plates in bending using strain
505 gradient theory, *Composites Part B: Engineering* (2019) 107006.

506 [52] J. Reddy, *Mechanics of Laminated Composite Plates and Shells: Theory*
507 *and Analysis, Second Edition*, CRC Press, 2004.

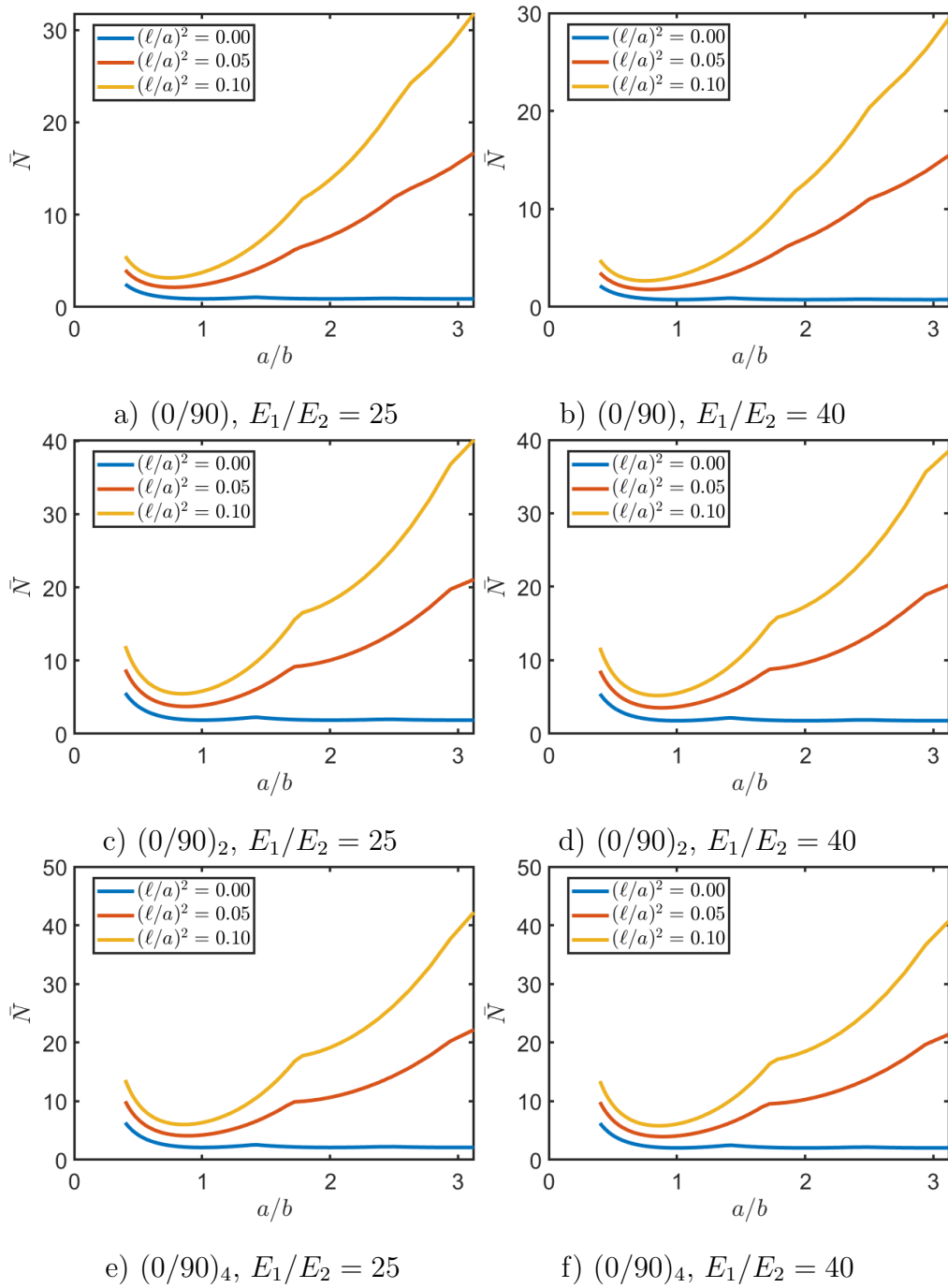


Figure 4: Uniaxial buckling load versus aspect ratio

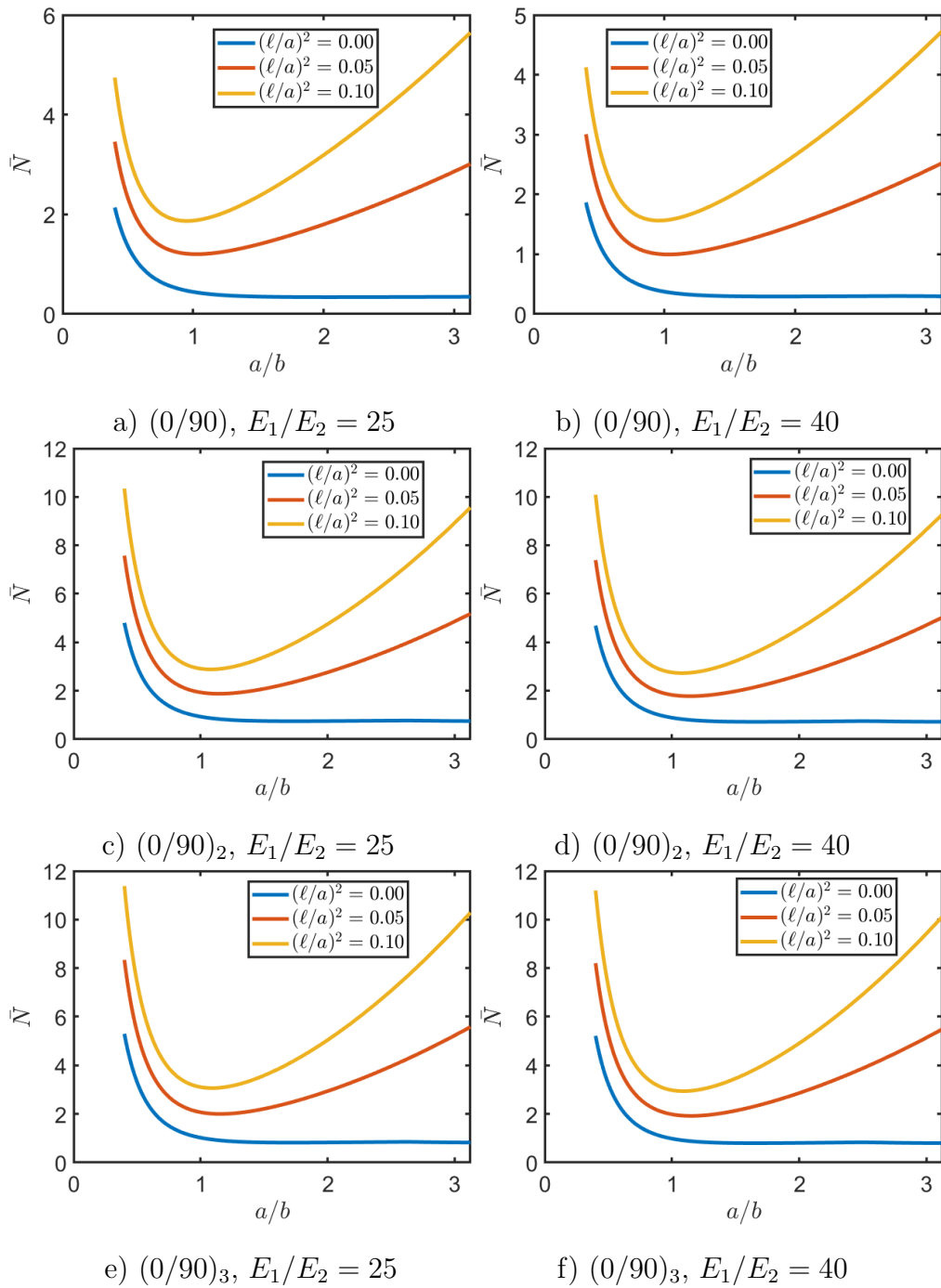


Figure 5: Biaxial buckling load versus aspect ratio

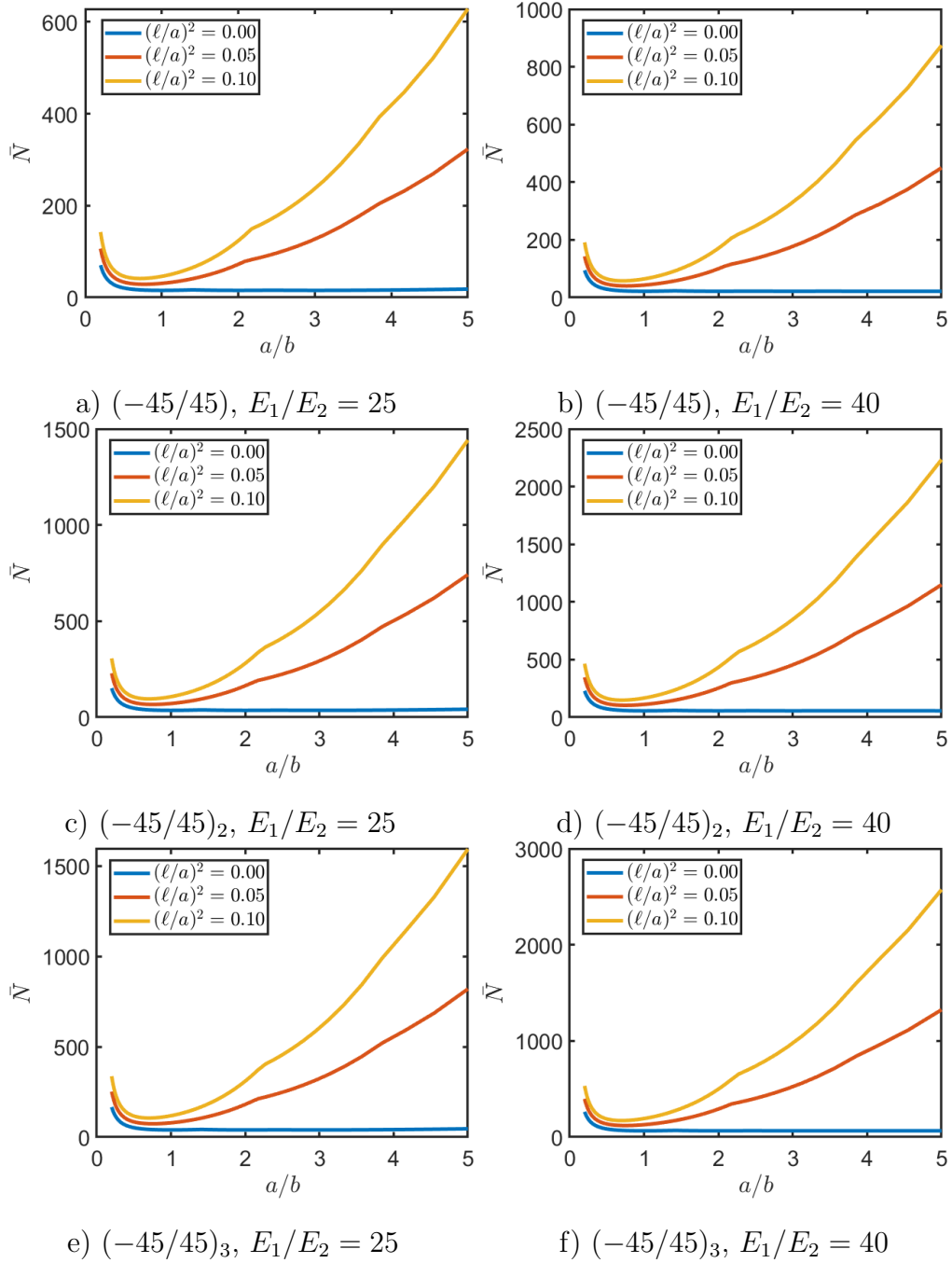


Figure 6: Uniaxial buckling load versus aspect ratio

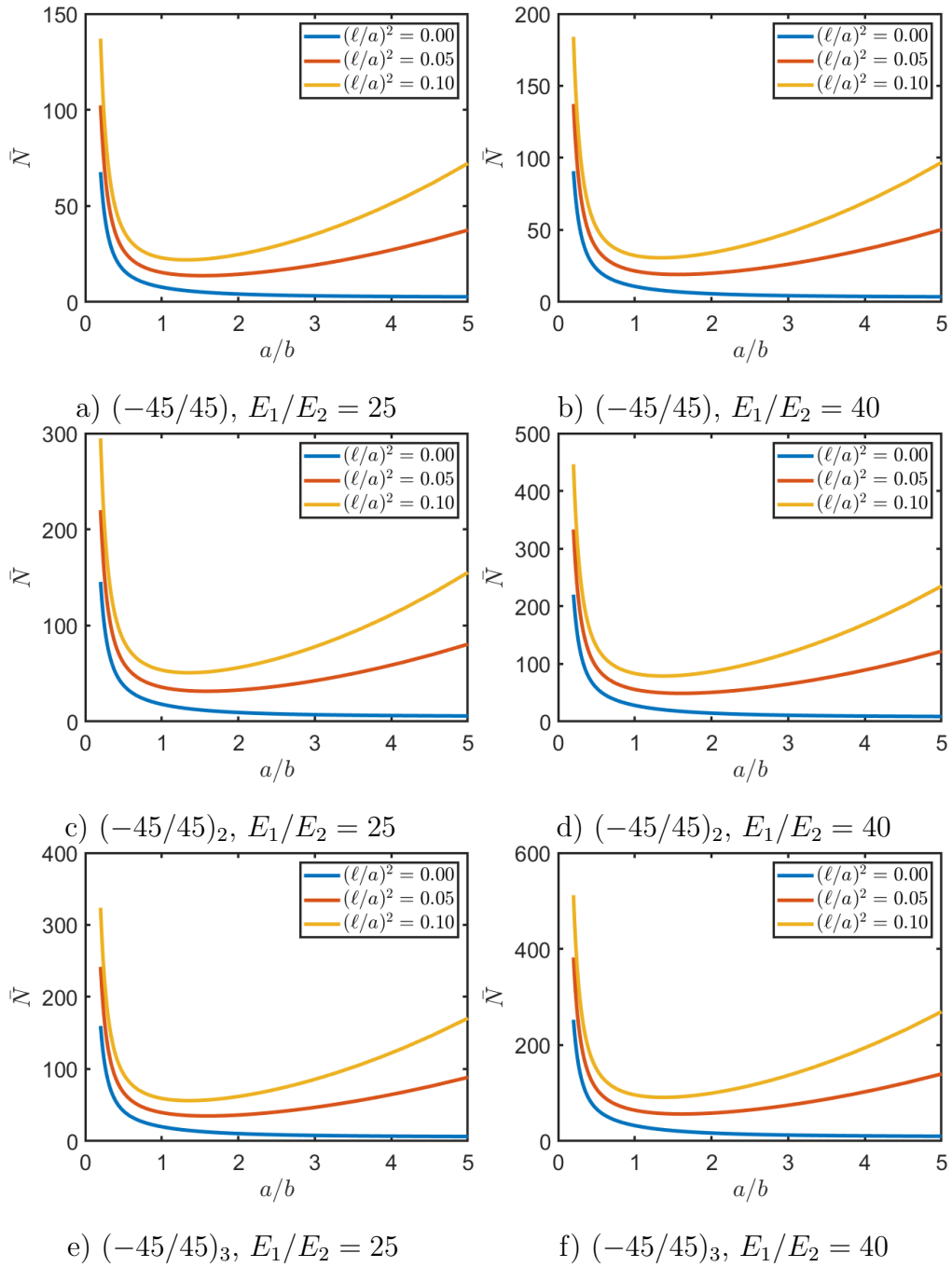


Figure 7: Biaxial buckling load versus aspect ratio

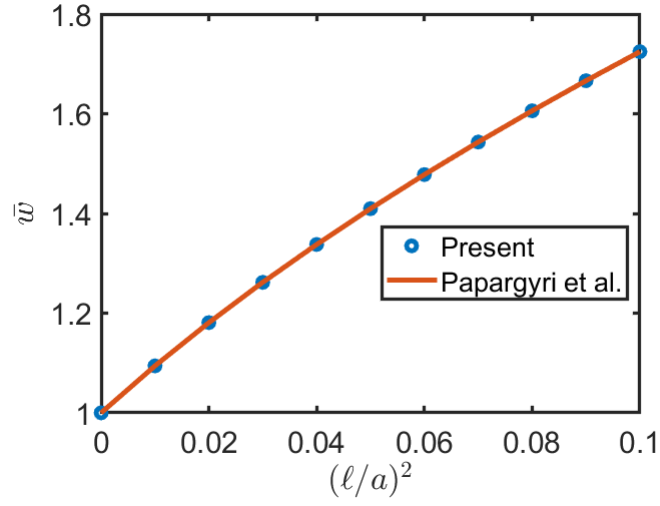


Figure 8: Vibrations - comparison with ref. [50].

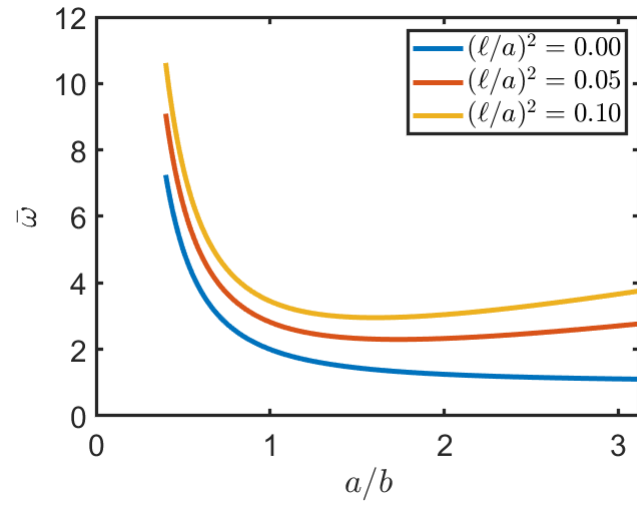


Figure 9: Nondimensionalized fundamental frequency load versus plate aspect ratio for isotropic lamina

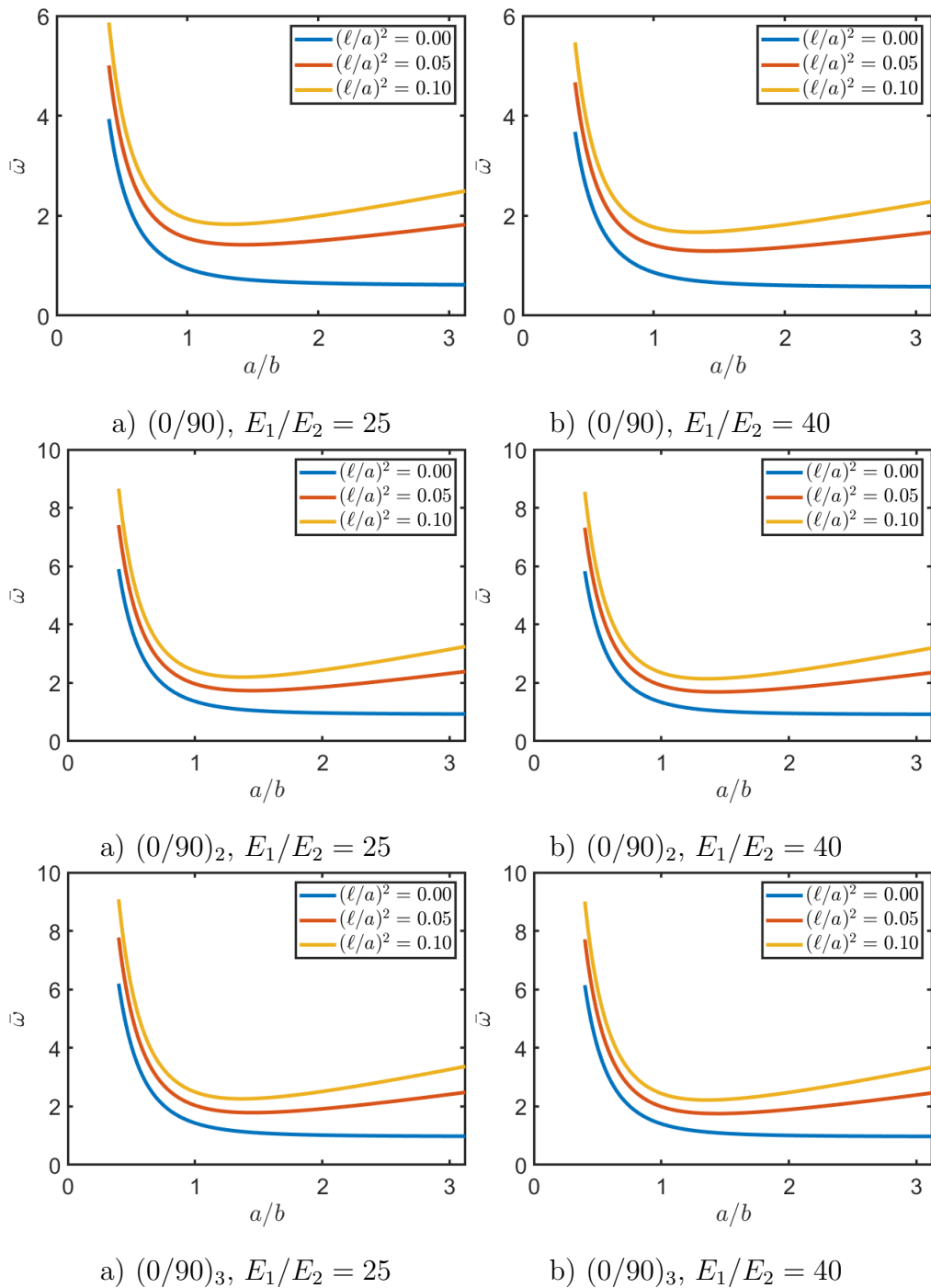


Figure 10: Dimensionless fundamental frequency versus plate aspect ratio for antisymmetric cross-ply laminates to changing non local ratios

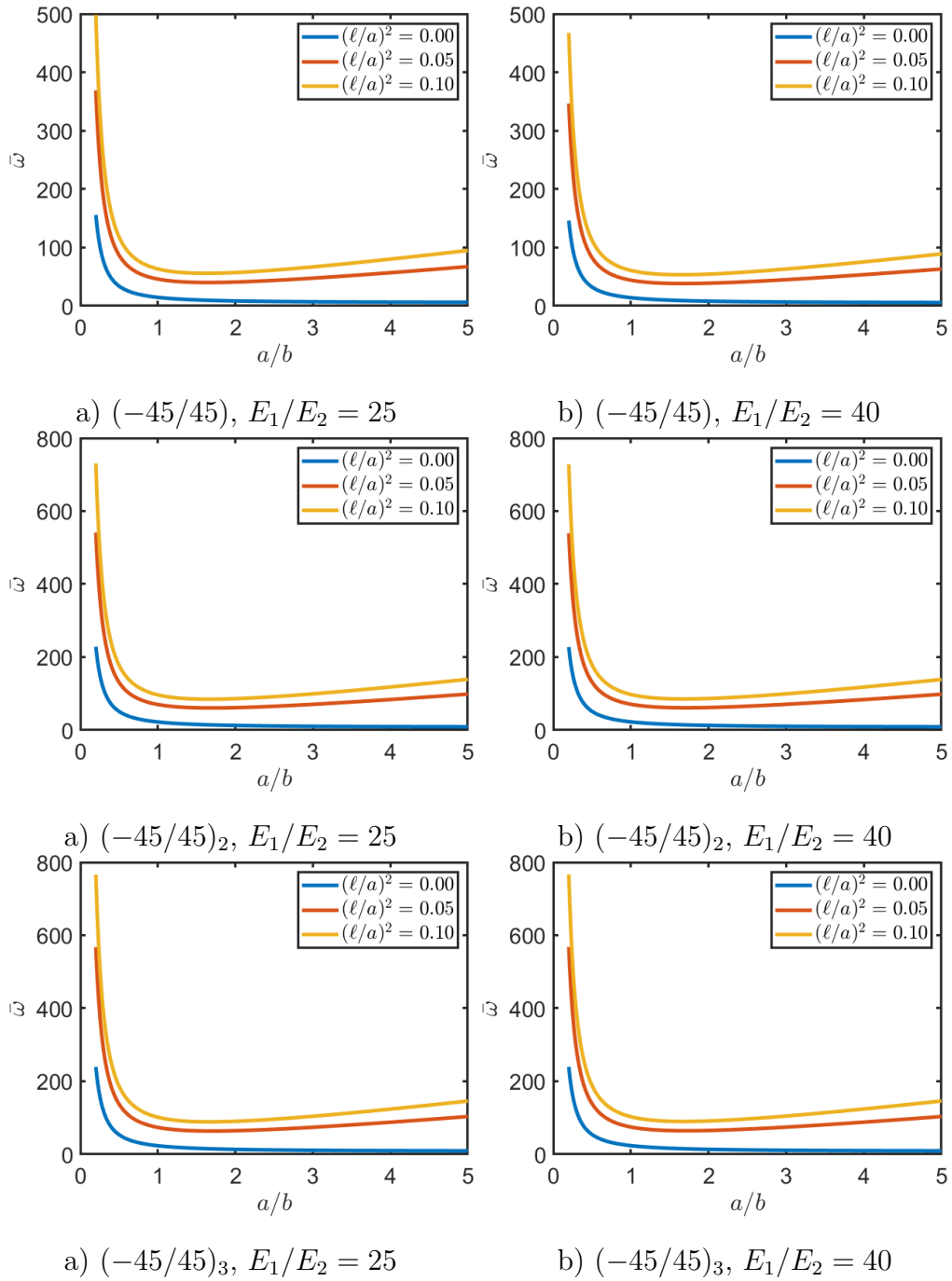


Figure 11: Dimensionless fundamental frequency versus plate aspect ratio for antisymmetric angle-ply laminates to changing non local ratios